Optical Engineering

OpticalEngineering.SPIEDigitalLibrary.org

Optical system design of four-channel dual-band infrared panoramic imaging

Gao Ming
Chen Yang
Zhang Xibin

SPIE.

Gao Ming, Chen Yang, Zhang Xibin, "Optical system design of four-channel dual-band infrared panoramic imaging," *Opt. Eng.* **58**(4), 045104 (2019), doi: 10.1117/1.OE.58.4.045104.

Optical system design of four-channel dual-band infrared panoramic imaging

Gao Ming,[a,*] Chen Yang,[a,*] and Zhang Xibin[b]
[a]Xi'an Technological University, School of Optoelectronic Engineering, Xi'an, China
[b]Xi'an Institute of Optics and Precision Mechanics, Testing Technology Service Center, Xi'an, China

Abstract. In order to reduce the volume of a panoramic optical system, a four-channel infrared dual-band panoramic imager was designed using spatial multicamera image mosaicking. Each optical system of the imaging channel was designed in a double imaging configuration with an *F*-number of 2, working bands of MWIR 3 to 5 μm and LWIR 8 to 12 μm, and a full field of view (FOV) of 122 deg. By adopting refractive-diffractive hybrid optical elements and introducing aspheric designs, the system was made to achieve temperature compensation from −40°C to 60°C by means of optical passive athermalization. Results indicate that the system attained almost 100% cold stop efficiency. At the Nyquist frequency of 18 lp/mm, the modulation-transfer-function (MTF) of the MWIR system was higher than 0.70 at the edges of the FOV, whereas the MTF of LWIR system was greater than 0.35 for the same condition, both approaching the diffraction limit. [DOI: 10.1117/1.OE.58.4.045104]

Keywords: cold optical system; infrared dual-band; panoramic imaging; passive athermalization; narcissus.

Paper 181550 received Nov. 3, 2018; accepted for publication Mar. 8, 2019; published online Apr. 27, 2019.

1 Introduction

With advancements in infrared (IR) detection technology, there is an increasing demand for high-performance optical systems, especially in modern military reconnaissance and space applications. Rapid target detection, real-time tracking, and accurate target measurement have become a major focus in the development of optical systems.[1] Currently, most of the existing automotive systems achieve a 360-deg panorama in the horizontal direction by mechanical rotation of a platform. In order to ensure the desired scan rate, dwell time on each pixel is only tens of microseconds, resulting in reduced signal-to-noise ratio (SNR) which causes delays between detection and target judgment.[2] Particularly, when capturing fast moving targets, the scanning system can be incapable of accurate searching and tracking, resulting in the loss of useful real-time target information.

HGH infrared system designed a type of IR 360-deg panoramic alert infrared camera which can capture photos at 360 deg azimuth and 20 deg vertical viewing angle. Raytheon developed an airborne distribution infrared sensor[3] and used six identical sensors with 90 deg field angle each, and installed them around the joint strike fighter to provide full range coverage. Thales Optronique limited company researched a type of ARTEMIS IRST (Infrared Search and Track) named "Moon Goddess" where the system was designed using a distributed sensor structure.[4] The three sensors contained FPA composed to realize the panoramic imaging (PI) of azimuth 360 deg and 25 deg elevation angle, with no blind spots in the imaging area. PI with 360 deg azimuth and 90 deg elevation angles was made possible with a five-channel panoramic optical system employing five spatially distributed objective lenses, each exceeding an FOV of 90 deg.[5,6]

*Address all correspondence to Gao Ming, E-mail: minggao1964@163.com; Chen Yang, E-mail: 867549558@qq.com

In this work, we present a four-channel dual-band IR PI optical system based on spatially distributed multiple lenses to capture scenes at different angles which are then combined to form a panorama. A double imaging configuration was incorporated into the system that resulted in a large aperture, increased field of view (FOV), and high resolution. Optical aberration was suppressed in 3 to 5 μm MWIR and 8 to 12 μm LWIR bands and the proposed system exhibited fast target search and tracking capabilities.

2 General Design of Panoramic System

2.1 *Working Concept*

PI is achieved using specialized imaging devices to obtain a hemispheric FOV of more than 180 deg in the vertical and horizontal direction of 360 deg FOV.[7] In order to acquire a full range of IR image data, the proposed design incorporates three IR objective lenses to divide the horizontal FOV for ensuring the integrity of data for two adjacent field parts, considering that fields of view of two adjacent lens need certain overlap. For that reason, the infrared lens field of each imaging channel is set to 122 deg, and then a complete PI system is obtained by splicing the images for all directions.

Three IR objective lenses in the horizontal direction receive the detected target information with different FOV. After transferring this information to the imaging system, detected light waves of various channels reach the focal plane array. Finally, after subsequent image splicing and matching, the panoramic image is displayed on a suitable display device. This process is shown in Fig. 1.

2.2 *Structural Design of the Panoramic System*

The structure and deployment of IR in a panoramic system is critical for producing high quality panoramic images.[5] Panoramic systems consist of an IR objective system, a transferring image optical system, an IR receiver lens and

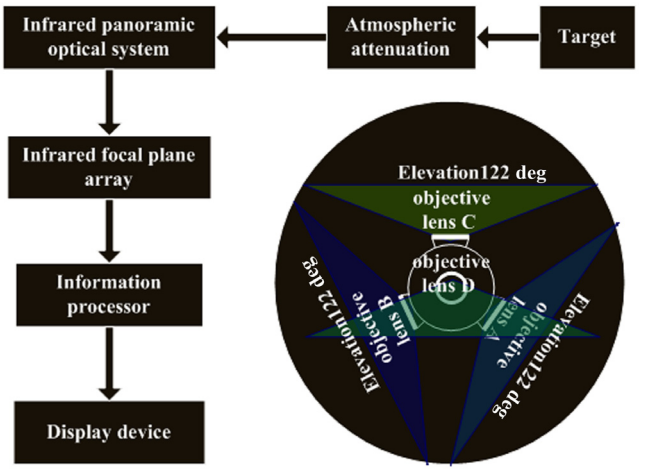

Fig. 1 The imaging principle of IR panoramic system.

detectors. A cobeam prism cemented together with the four right-angle prisms lies in the center position of the sphere. The four flat mirrors are denoted by M1, M2, M3, and M4. Optical path 1 enters the system from the objective lens A and arrives at the beam splitter prism after one reflection on the cobeam prism; optical path 2 enters the system from the objective lens B, arrives at the cobeam prism after two reflections from mirrors M1 and M2, and then reaches the beam splitter prism after another reflection; optical path 3 enters the system from the objective lens C, arrives at the partially reflecting mirror after reflections from mirrors M3 and M4, and then passes through the beam splitter prism after the cobeam prism; optical path 4 enters the system from objective lens D, through the partially reflecting mirror and the cobeam prism, and then arrives at the beam splitter prism. MWIR and LWIR are separated using the beam splitter, making images on two high-resolution IR detection focal planes IFPD1 (infrared focal plane array) and IFPD2, respectively. Thereby, a complete panoramic image is created by splicing subsequent images. The four IR lenses are designed according to the common path structure so that the system can respond to MWIR and LWIR bands simultaneously. On the one hand, this system design avoids the need to switch lenses since the optical paths of the lenses are common, and also makes the system more compact. On the other hand, the system can fully exploit the benefits of MWIR and LWIR to meet the practical application needs (Fig. 2).

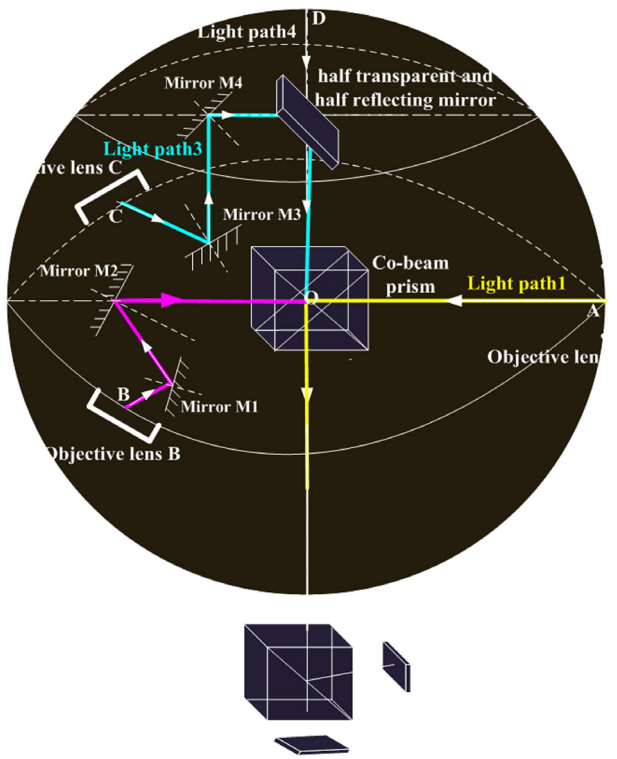

Fig. 2 Structural representation of the panoramic system.

3 Design Approach of Optical System

3.1 *Specifications of Optical System*

The pixel size and resolution of MWIR and LWIR detectors is 28 μm and 640×512 pixels, respectively. The specifications of the optical system, determined by detector models and practical considerations, are shown in Table 1.

3.2 *Structure Design of the Optical System*

The system adopts a hybrid refractive-diffractive structure, which can attain a larger FOV and meet our requirements. On the one hand, the introduction of the diffractive surfaces can weaken the vertical axis aberration and the chromatic aberration by taking advantages of unique dispersion characteristics of diffractive element; on the other hand, it can reduce the diameter of the system, making the system lightweight and portable.

It is necessary to consider the cold stop characteristics of the system itself with regard to a cooled IR system.[8] Cold stop determines the location and size of the exit pupil of the optical system. Attaining a 100% cold stop efficiency indicates that the exit pupil of the optical system is able to match the cold stop of the detector. Otherwise, there is a risk of beam cutting which can reduce the system sensitivity or cause additional incident hybrid heat radiation entering the detector, which in turn can reduce the SNR of system.

Wide-field imaging systems typically have short effective focal lengths. In order to ensure a sufficient working distance, our system uses a double imaging configuration design known as the quadratic imaging configuration. A single imaging system requires a large aperture of the cooled IR system in order to achieve 100% efficiency of cold stop. Therefore, adding a secondary imaging configuration behind the first imaging position can reduce the radial dimension of the system. Moreover, for the double imaging configuration system, the first configuration group burdens the major diopter of the system, and latter configuration mainly plays a part

Table 1 Optical design specifications.

	Workband	F#	FOV	Focal length	Requirements for image quality
MWIR	3 to 5 μm	2	122 deg	6.36 mm	MTF > 0.5
LWIR	8 to 12 μm				MTF > 0.3

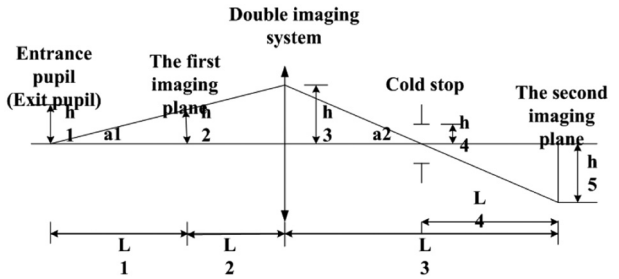

Fig. 3 Principal ray diagram of a double-band optical system.

in secondary imaging with the completion of residual aberration balance. The principal ray diagram of double imaging system is shown in Fig. 3.

In Fig. 3, L_4, h_4, h_5, a_1, a_2 have been identified. According to equation for a paraxial optical system

$$L_2 = \frac{f}{M} + f, \tag{1}$$

$$L_3 = ML_2. \tag{2}$$

In the above equation, M denotes the total lateral magnification of double imaging system. We can obtain the following relationships from the geometrical arrangement shown in Fig. 3:

$$\tan a_1 = \frac{h_2}{L_1}, \tag{3}$$

$$\tan a_2 = \frac{h_5}{L_4}, \tag{4}$$

$$T = \frac{\tan a_2}{\tan a_1}, \tag{5}$$

$$h_3 = (L_3 - L_4)\tan a_2, \tag{6}$$

$$h_3 = (L + L_2)\tan a_1, \tag{7}$$

$$h_3 = L_2 \tan a_1 + \frac{h_5}{M}. \tag{8}$$

Combining with the equations from Eqs. (1)–(9), L_3 can be derived as follows:

$$L_3 = \frac{-ML_4T - \frac{h_5}{\tan a_1}}{1 - MT}. \tag{9}$$

From these results, we can deduce that: (1) the distance from exit pupil to the final image surface shortens with the included angle between the principal ray and the optical axis gradually decreasing, which affects the aberration unfavorably. In order to achieve 100% cold stop efficiency, it needs to coincide with aperture stop of the system. This is required for eliminating stray light and ensuring that the detector detects only the image in its FOV. (2) With the increase of axial magnification of the double imaging system, spacing from the exit pupil to the final image surface gradually decreases. Although this can make the system more compact, the F number of the system can increase, should be avoided.

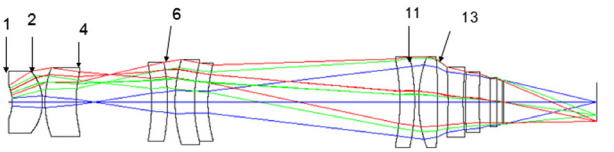

Fig. 4 Initial structure of signal IR objective optical system.

4 Design Results and Image Quality Evaluation of Optical System

4.1 *System Design*

Figure 4 shows the optical arrangement for the proposed MWIR/LWIR dual-band panoramic system, with an FOV of 122 deg and the F number equivalent to 2. A hybrid refractive-diffractive structure was employed in the design. Optical surfaces marked with numbers 1, 6, and 11 are aspheric, surfaces 2, 4, and 13 are diffractive, while the remaining surfaces are spherical. IR materials such as ZnSe, ZnSe, and ZnS were chosen to match, with the total length of system set to 220 mm.

Surfaces 1, 6, and 11 are even, while 2, 4, and 13 are binary aspheric. One of the imaging channels of the IR dual-band panoramic system is shown in Fig. 5. Each imaging channel contains two configurations of MWIR and LWIR, a coaperture, a cobeam a prism, a beam splitter prism, a receiving objective lens of IR detector, and a focal plane of MWIR and LWIR. Dual-band coaperture form is applied in the former configuration of IR objective lens to achieve the synchronized imaging of MWIR and LWIR without the need for a switching mechanism.

Five lenses were used in the coaperture design of the system. The cobeam prism in the middle was composed of four identical isosceles right angle prisms that were mutually glued together at the oblique side coated with a semi-reflective film. Antireflection film was coated on the surfaces of rectangular prism, to minimize any loss of the incident radiation. According to the transmittance of half transparent half reflecting mirror and cobeam prism is 50%, and the beam splitter will not attenuate energy, which splitting wavelength rather than splitting energy, it can be estimated that the transmittance of light path 1 and 2 is about 50%, and the light path 3 and 4 is about 25%. Four lenses were used in the IR detector objective lens, for allocating the optical diopter of system and balancing the overall system aberrations. Ge, ZnSe, and ZnS satisfy the required physical and chemical properties. They were selected according to their refractive indexes and Abbe numbers for achromatism and athermalization.

4.2 *Image Quality Evaluation*

4.2.1 *Modulation-transfer-function*

In this optical system, image quality of light path 1 is similar to that of light path 4, with light paths 2 and 3 also having similar image quality.

In light paths 1 and 4, from the modulation-transfer-function (MTF) analysis of MWIR and LWIR shown in Figs. 6(a) and 6(b), it can be observed that the MTF values are all close to the diffraction limit at the Nyquist frequency of 18 lp/mm. The MTF of MWIR > 0.72 and the MTF of LWIR > 0.45, satisfying the requirements of imaging quality.[9]

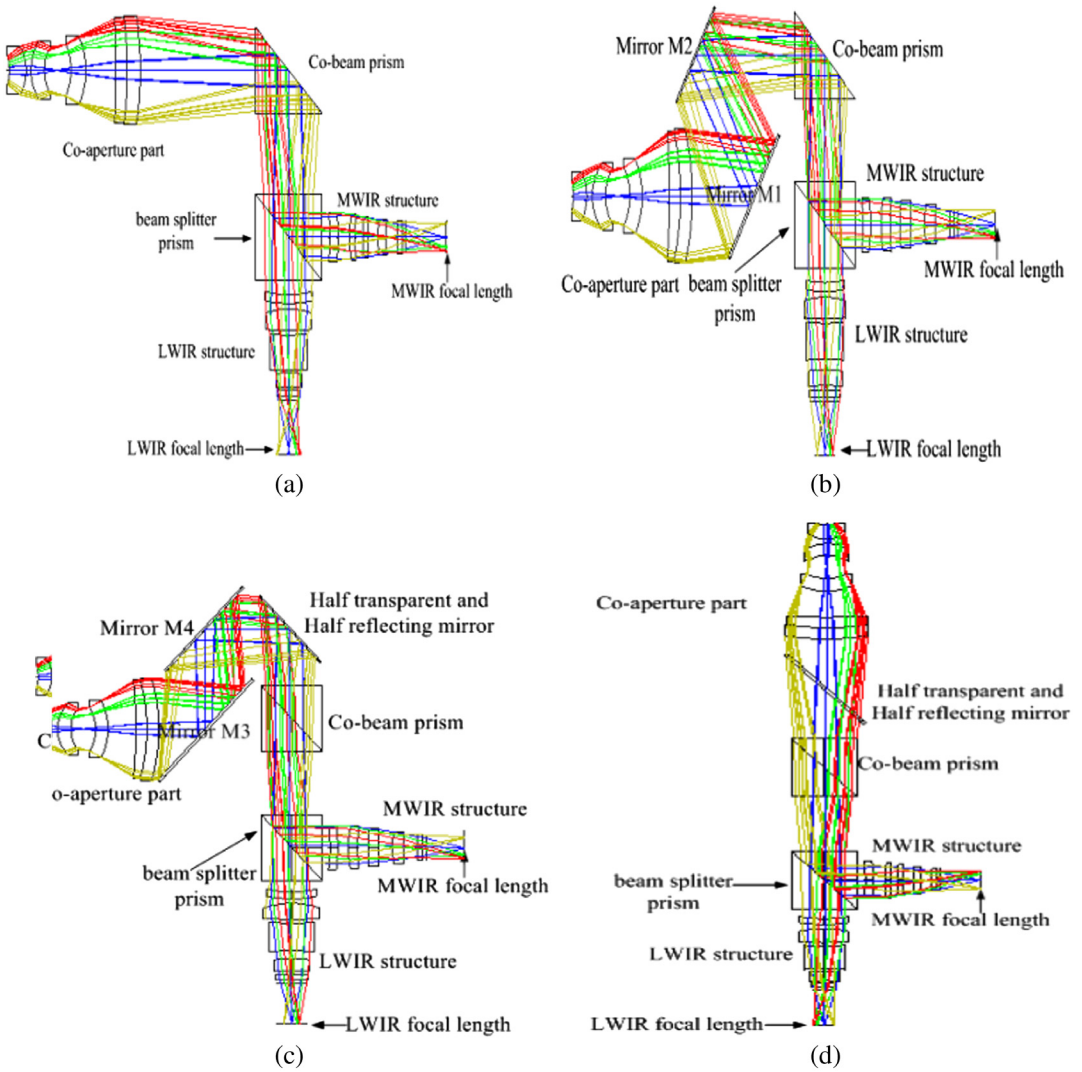

Fig. 5 Structure of the dual-band co-aperture optical system. (a) Light path 1, (b) light path 2, (c) light path 3, and (d) light path 4.

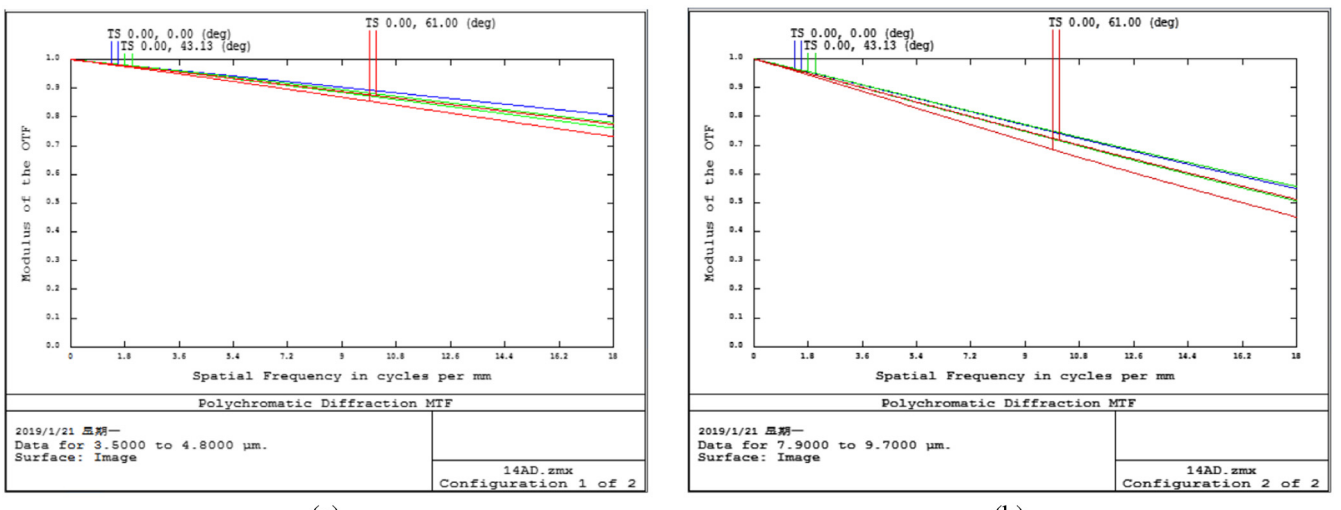

Fig. 6 The MTF of light paths 1 and 4. (a) MWIR and (b) LWIR.

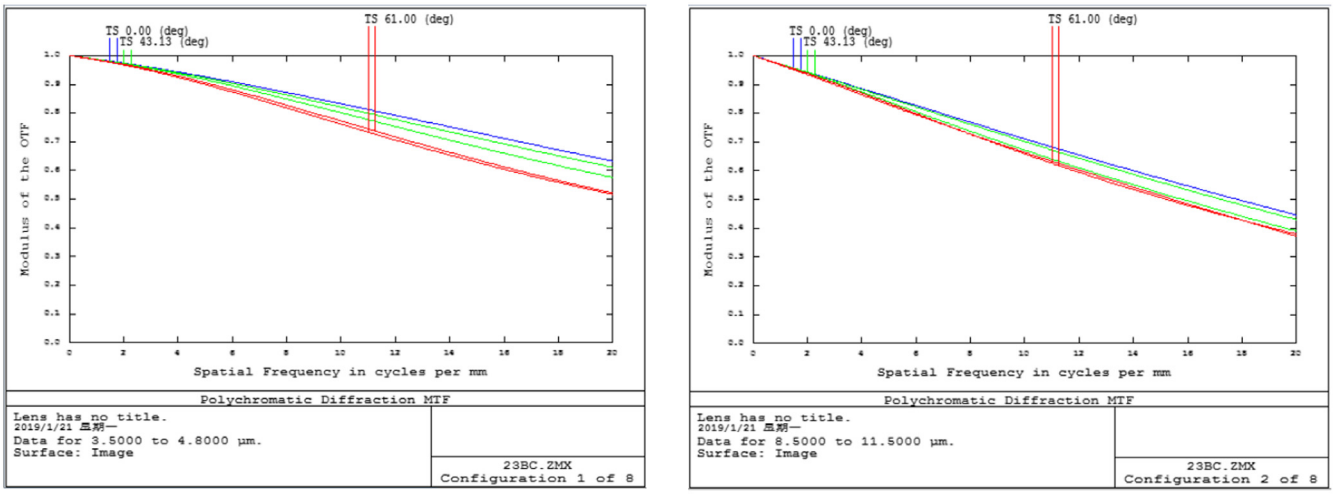

(a) (b)

Fig. 7 The MTF of 2 and 3 light path. (a) MWIR and (b) LWIR.

The MTF analysis of MWIR and LWIR for light paths 2 and 3 is shown in Figs. 7(a) and 7(b). It can be seen that the MTF is higher than 0.70 in MWIR and 0.35 in LWIR, at the Nyquist frequency of 18 lp/mm.

4.2.2 *Energy distribution and calculation*

The energy distribution of the light spot along with radial variations of light paths 1 and 4 can be obtained from Zemax software, as shown in Fig. 8. It can be seen that the energy concentration rate within a single pixel reached ∼85% and 75% under the full FOV for MWIR and LWIR, respectively.

The energy concentration rate of light focused on Fig. 9 shows the light spot energy distribution of MWIR and LWIR along with radial variations for light paths 2 and 3. It can be seen that the energy concentration rate within one pixel size reached ∼80% and 63% under the full FOV for MWIR and LWIR systems, respectively.

Although the energy concentration rate of light focused on the detector focal plane can reach above 75% ideally, the optical system exhibits energy losses mainly due to three effects: (a) reflection loss of MWIR and (b) absorption loss of LWIR.

4.2.3 *Detection blind area range calculation*

Figure 10 shows the detection blind area range schematic of the PI system. The system uses the A, B, and C IR lenses to divide the horizontal FOV, achieving 360 deg PI in the horizontal direction. Each IR lense has an FOV of 122 deg, so that the detection FOV of two adjacent lens has overlaps in the horizontal direction in order to ensure a complete panoramic image. A blind area denoted by AOCH exists where all IR lenses are incapable of detecting. O denotes the center point of the system, and A, B, and C denote the entrance pupil centers of the IR lenses. From the design parameters, it follows that AO = 136.241 mm.

The geometric relations are given as

$$\frac{\sin\angle AOH}{AH} = \frac{\sin\angle AHO}{AO}. \tag{10}$$

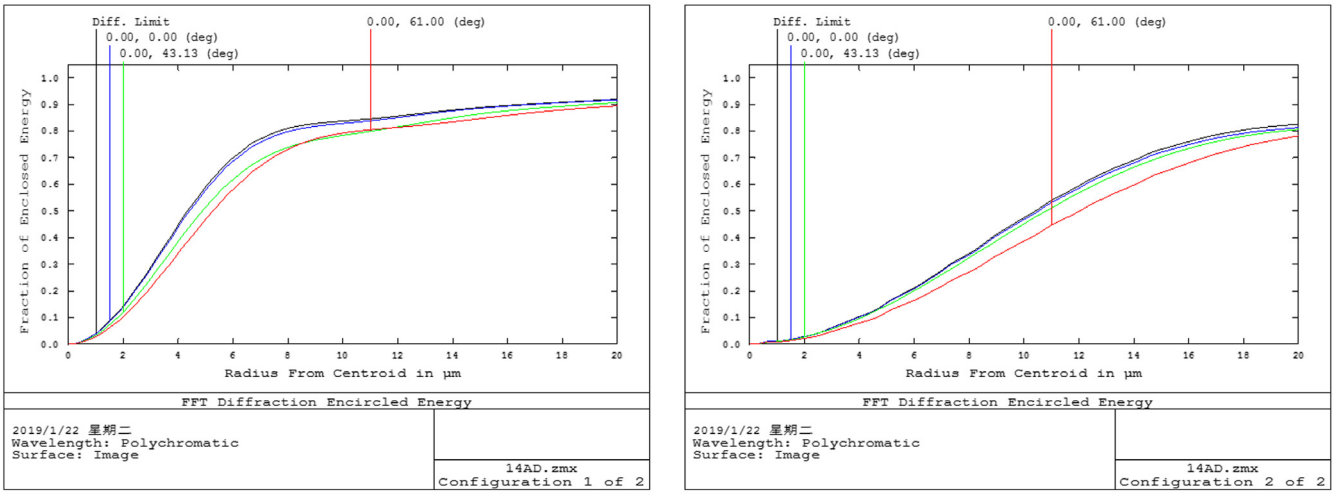

(a) (b)

Fig. 8 Energy distribution of optical paths 1 and 4. (a) MWIR and (b) LWIR.

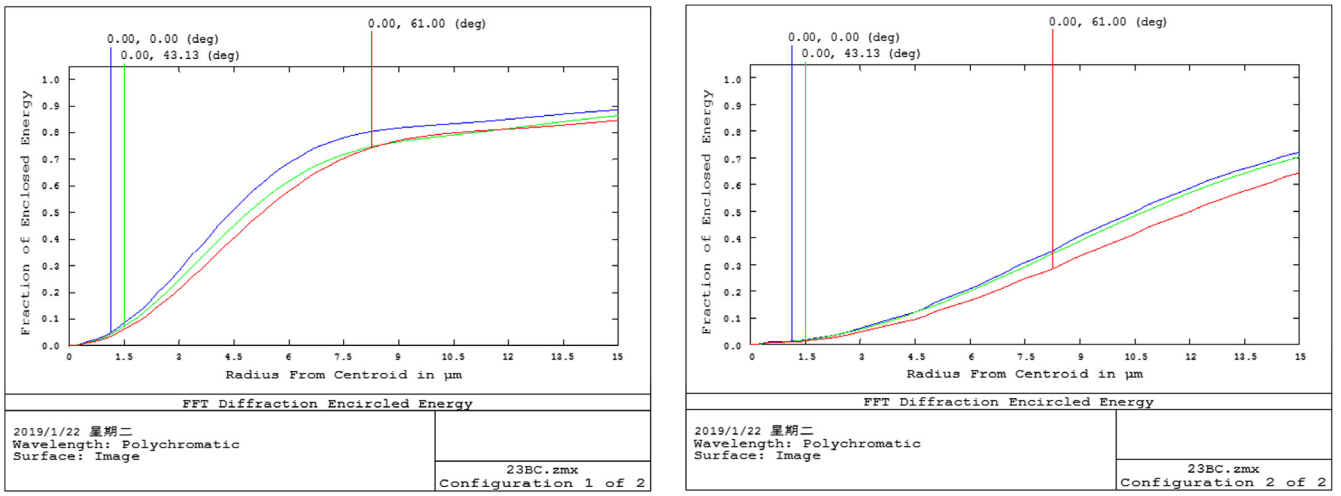

(a) (b)

Fig. 9 Energy distribution of the optical system. (a) MWIR and (b) LWIR.

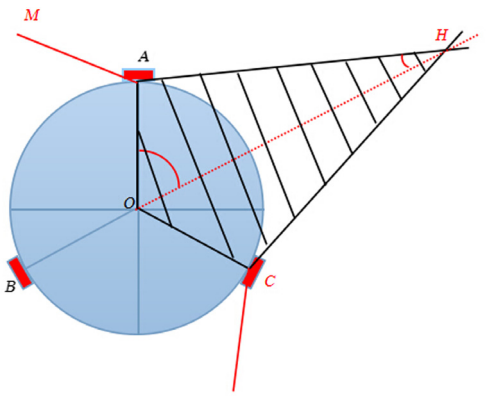

Fig. 10 Detection blind area range of the panoramic system.

From this relationship AH is found to be 6.760 m. Evidently, if the horizontal direction 360 deg FOV is divided between the three IR lenses, the target can evade detection when it enters the range within about 6.76 m. This structure with three IR lenses in the horizontal direction and one IR lens in the vertical axis direction constitutes the four-channel PI system. This approach remarkably reduces the volume and weight of the system, while meeting the design requirements.

4.2.4 *Cold stop analysis*

In order to achieve 100% cold diaphragm, the pupil position and size of the optical system are required to be the same as that of the cold diaphragm of the refrigeration detector. It is known that the cold diaphragm of the detector is 25 mm in front of the photosensitive surface, and its diameter is 12.5 mm. The optical system has a pupil distance of 25 mm and a diameter of 12.5 mm. It matches the detector cold aperture perfectly and meets 100% cold aperture effect.

5 System Athermalization and Narcissus Analysis

5.1 *Optical Passive Athermalization*

Athermalization has to be considered in the system in order to account for ambient temperature changes that affect the refractive index, thickness, interval, and the radius of curvature for IR materials. The system is analyzed in the −40°C to 60°C temperature range in order to find the dependence of defocus on temperature of the two bands, with the goal of eliminating defocus by compensating through athermalization. For achieving passive optical athermalization, the thermal expansion coefficient and the dispersion factor need to meet the following criteria:[10]

$$\begin{cases} \left(\frac{1}{h_1\psi}\right)^2 \sum_{i=1}^{n} (h_i^2 \eta_i \psi_i) = 0 \\ \left(\frac{1}{h_1\psi}\right)^2 \sum_{i=1}^{n} (h_i^2 \chi_i \psi_i) + \alpha_j L = 0 \end{cases}, \tag{11}$$

where h_i is the height of the paraxial rays at the lens number i; Ψ is the dioptry of system; Ψ_i is the dioptry of the number i lens; n_i is the dispersion factor of lens; χ_i is the thermal expansion coefficient; a_j is the thermal expansion coefficient of the barrel mechanical structure; and L is the barrel length. From Eq. (11), it follows that passive athermalization of the system can be achieved when the dispersion defocus is equal to zero and the thermal defocus of the lens offsets that of the mechanical structure. Diffractive elements are incorporated in the design for the purpose of simplification. Diffraction and the thermal expansion coefficient of the refractive lens are be given by the following expression:[11]

$$\begin{cases} C_d = 2\alpha_g + \frac{1}{n_0}\frac{dn_0}{dt} \\ C_r = \alpha_g - \frac{1}{n-n_0}\left(\frac{dn}{dt} - n\frac{dn_0}{dt}\right) \end{cases}, \tag{12}$$

where a_g is the thermal expansion coefficient of lens; n and n_0 denote the refractive index of the lens and the media, respectively; dn/dt and dn_0/dt represent the refractive index temperature coefficient of the material and the medium, respectively. It can be seen that the temperature characteristic of diffractive elements depends solely on the thermal expansion coefficient of the materials. Therefore, introducing the optimal diffractive surfaces can accomplish athermalization. Due to spatial considerations, only the analysis of the athermal difference of light path 1 is given here.

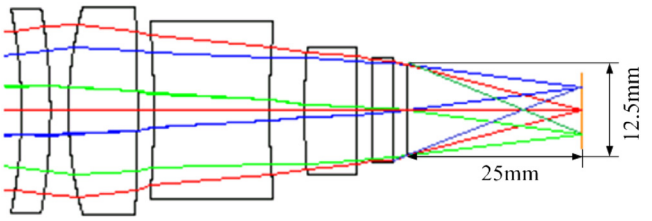

Fig. 11 Exit pupil of optical system.

Figures 11 and 12 denote the MTF of MWIR and LWIR systems at the temperature of −40°C, 20°C, and 60°C, respectively. It can be seen that for all temperatures, the MTF values for the MWIR and LWIR systems at the Nyquist frequency of 18 lp/mm are greater than 0.6 and 0.4, respectively. This indicates that the image quality meets the design requirements after athermalization.

5.2 *Narcissus Analysis*

Narcissus is the self-image of "cold light" emitted from the focal plane of the cooled IR detector. It is formed when the IR radiation passes the surface reflection of system lenses and then refocuses on the focal plane. Besides the detected target information, the detector also receives its own image, thereby seriously affecting the sensitivity of the system. Hence, during the design process of a cooled IR optical system, narcissus phenomenon has to be considered.[11] Typically, YNI value is used to characterize the amount of narcissus, where Y is the incident height of paraxial rays on one optical surface, N is the refractive index of one optical material, and I is the incident angle of marginal rays at one optical surface. If the YNI value is greater than 1, it indicates that the impact of narcissus to the optical system can be ignored. For values of YNI below 1, further analysis is required.

Due to the limitation of space, the analysis of the narcissus of the 1 light path is given. The YNI values are shown in Table 2.

It can be seen from Table 2, the YNI value of surfaces 5, 7, 19 is less than 1, so it needs to undergo reverse ray tracing analysis, as shown from Figs. 13(a)–13(c).

It can be seen from Figs. 13(a)–13(c) that the reflected light from the 5th, the 7th, and the 19th surface is diverging and cannot reach the IR focal plane, hence it can be ignored. Comprehensive analysis shows narcissus does not affect the image quality of the optical system (Fig. 14).

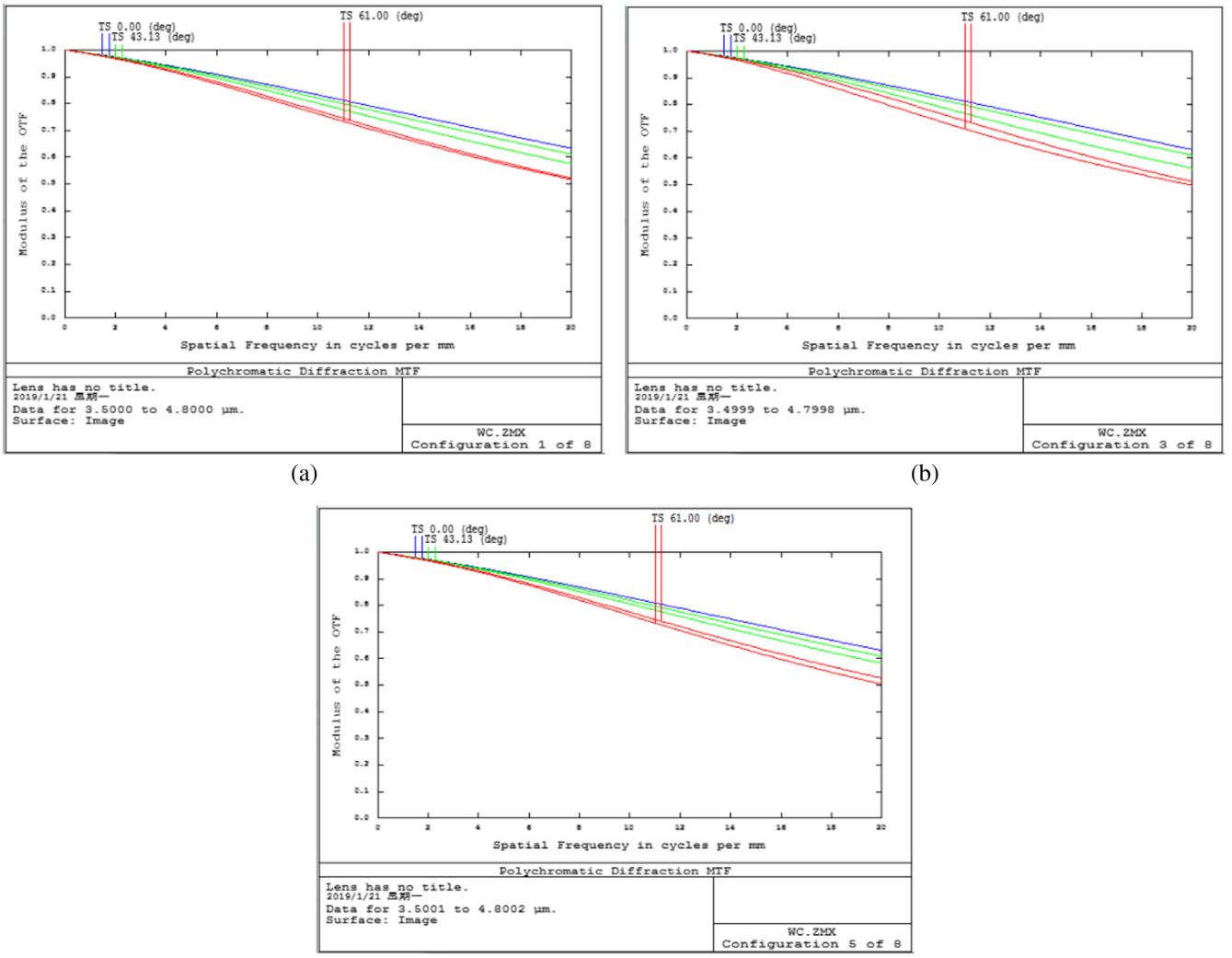

Fig. 12 The MTF of MWIR after athermalization. (a) −40°C, (b) 20°C, and (c) 60°C.

Table 2 YNI contribution value of 1 light path.

Surface number	YNI	Surface number	YNI	Surface number	YNI
1	−2.1192	2	−2.4274	3	−1.01395
4	−1.8181	5	0.9789	6	1.0917
7	0.3746	8	1.6793	9	3.4286
10	2.2687	11	1.3889	12	−1.0241
13	−3.8548	14	2.6913	15	−2.9996
16	−5.1189	17	−1.4699	18	−1.3313
19	0.5360	20	−1.6452	21	−1.5202

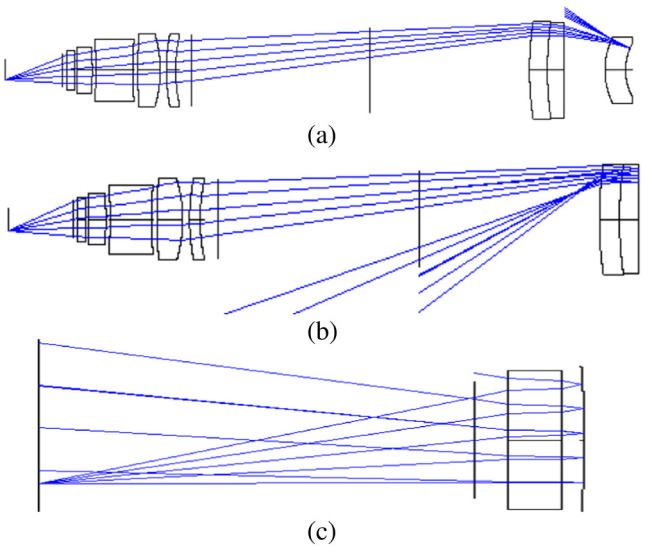

Fig. 14 Narcissus analysis of optical path 1. (a) Reverse ray tracing schematic of fifth surface. (b) Reverse ray tracing schematic of seventh surface. (c) Reverse ray tracing schematic of 19th surface.

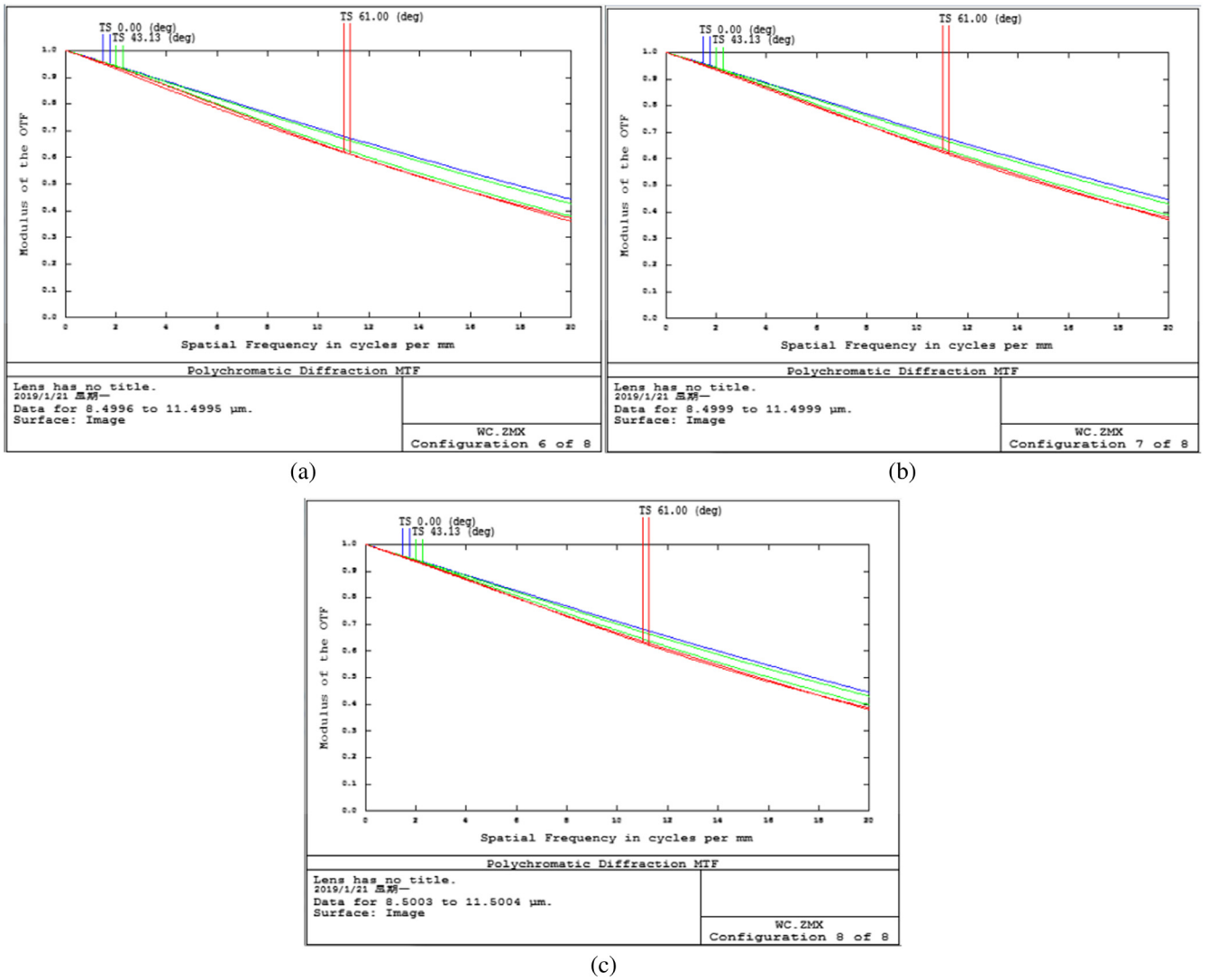

Fig. 13 The MTF of LWIR after athermalization. (a) −40°C, (b) 20°C, and (c) 60°C.

6 Conclusion

A cooled, high-resolution, four-channel IR dual-band PI optical system was designed with spatially distributed multiple lenses. It was composed of MWIR/LWIR IR dual-band coaperture objective lenses and a double imaging structure. The design optimized relative apertures, FOV, and focal lengths and was capable of image fusion in IR dual-band while achieving 100% cold stop efficiency. IR materials such as Ge, ZnSe, and ZnS were combined with aspheric and diffractive surfaces to ensure excellent imaging quality of the system and stability in the −40°C to 60°C temperature range. The system has the advantages of a large relative aperture, large FOV, excellent image quality, high-resolution, thermal sensitivity, small size, and light weight. The compact

Table 3 The first configuration of BD channels.

Surf:type	Radius	Thickness	Glass
Standard	Infinity	Infinity	
Standard	−17.479	8.278	GERMANIUM
Standard	−18.517	9.857	
Standard	42.812	6.365	AMTIR1
Binary 2	55.386	2.13	
Standard	52.731	6.067	ZNSE
Even aspheric	38.048	8.741	
Standard	−33.365	5.677	GERMANIUM
Even aspheric	−36.196	29.015	
Standard	−246.151	11.415	TI_1173
Standard	−58.971	12.411	ZNS_BROAD
Standard	−92.2	181.14	
Standard	Infinity	15	GERMANIUM
Tilted		15	GERMANIUM
Standard	Infinity	44.455	
Standard	Infinity	12	GERMANIUM
Tilted		12	GERMANIUM
Standard	Infinity	32.08	
Standard	−57.571	5.091	GE_OLD
Even aspheric	−73.363	2.405	
Standard	53.572	12.278	ZNSE
Binary 2	−199.034	1.171	
Standard	−264.003	12.651	AMTIR1
Standard	286.834	3.191	
Standard	122.802	8.621	GE_OLD
Standard	189.181	3.511	
Standard	Infinity	2	GERMANIUM
Standard	Infinity	2	
Standard	Infinity	25	
Standard	Infinity	—	

Table 4 The second configuration of BD channels.

Surf:type	Radius	Thickness	Glass
Standard	Infinity	Infinity	
Standard	−17.479	8.278	GERMANIUM
Standard	−18.517	9.857	
Standard	42.812	6.365	AMTIR1
Binary 2	55.386	2.13	
Standard	52.731	6.067	ZNSE
Even aspheric	38.048	8.741	
Standard	−33.365	5.677	GERMANIUM
Even aspheric	−36.196	29.015	
Standard	−246.151	11.415	TI_1173
Standard	−58.971	12.411	ZNS_BROAD
Standard	−92.2	181.14	
Standard	Infinity	15	GERMANIUM
Tilted		15	GERMANIUM
Standard	Infinity	44.455	
Standard	Infinity	12	GERMANIUM
Tilted		12	GERMANIUM
Standard	Infinity	32.08	
Standard	Infinity	−2.469	GERMANIUM
Standard	85.672	−3.186	
Even aspheric	103.011	−2	
Standard	−52.635	−2.01	AMTIR3
Binary 2	−122.128	−6	
Standard	−3087.62	−2	IG2
Standard	9495.896	−4.141	
Standard	−95.594	−13.446	IRG205
Standard	−237.658	−7.588	
Standard	Infinity	−2	GERMANIUM
Standard	Infinity	−2	
Standard	Infinity	−25	
Standard	Infinity	–	

and improved panoramic IR imaging system described in this work is promising for broad applications in IR search and tracking identification.

7 Appendix of Lens Prescription

The B and D channels are common light path channels, which are the parameters of the first configuration of the lens (Table 3).

Table 5 The first configuration of AC channels.

Surf:type	Radius	Thickness	Glass
Standard	Infinity	Infinity	
Standard	−13.21	5.993	GAAS
Standard	−12.869	4.999	
Standard	25.992	9.328	AMTIR1
Binary 2	36.76	1.498	
Standard	62.588	5.243	ZNSE
Even aspheric	34.071	5.007	
Standard	−43.452	9.921	IG2
Even aspheric	−43.299	33.709	
Standard	−1.22E + 04	8.537	CDSE
Standard	−81.209	19.191	ZNS_BROAD
Standard	−102.79	75	
Standard	Infinity	18	GERMANIUM
Tilted		18	GERMANIUM
Standard	Infinity	45.4	
Standard	Infinity	12	GERMANIUM
Tilted		12	GERMANIUM
Standard	Infinity	32.675	
Standard	−57.568	5.092	GE_OLD
Even aspheric	−73.369	2.395	
Standard	53.579	12.268	ZNSE
Binary 2	−199.253	1.169	
Standard	−263.886	12.631	AMTIR1
Standard	286.627	3.178	
Standard	122.825	8.613	GE_OLD
Standard	189.176	3.506	
Standard	Infinity	2	GERMANIUM
Standard	Infinity	2	
Standard	Infinity	25	
Standard	Infinity	–	

The B and D channels are common light path channels, which are the parameters of the second configuration of the lens (Table 4).

Both A and C channels are common light path channels, which are parameters of the first configuration of the lens (Table 5).

Table 6 The second configuration of AC channels.

Surf:type	Radius	Thickness	Glass
Standard	Infinity	Infinity	
Standard	−13.21	5.993	GAAS
Standard	−12.869	4.999	
Standard	25.992	9.328	AMTIR1
Binary 2	36.76	1.498	
Standard	62.588	5.243	ZNSE
Even aspheric	34.071	5.007	
Standard	−43.452	9.921	IG2
Even aspheric	−43.299	33.709	
Standard	$-1.22E+07$	8.537	CDSE
Standard	−81.209	19.191	ZNS_BROAD
Standard	−102.79	75	
Standard	Infinity	18	GERMANIUM
Tilted		18	GERMANIUM
Standard	Infinity	45.4	GERMANIUM
Standard	Infinity	12	
Tilted		−12	GERMANIUM
Standard	Infinity	Infinity	GE_LONG
Standard	Infinity	−2	
Standard	85.736	−3.208	
Even aspheric	102.992	−2.039	
Standard	−52.655	−2.022	AMTIR3
Binary 2	−122.067	−6	
Standard	−3141.085	−1.999	AGCL
Standard	9600.394	−4.044	
Standard	−95.664	−13.409	IRG205
Standard	−236.636	−7.579	
Standard	Infinity	−2	GERMANIUM
Standard	Infinity	−2	
Standard	Infinity	−25	
Standard	Infinity	–	

Table 7 The extra data.

		Norm radius		
Binary 2	12	−24.541	−14.539	3.908
Binary 2	14	−48.219	−6.402	26.873
Binary 2	29	−144.683	474.934	−8200.672

Both A and C channels are common light path channels, which are parameters of the second configuration of the lens (Tables 6 and 7).

Acknowledgments

This paper was supported by Army equipment pre-research project (Grant No. 301XXX102) and Key Laboratory of Shaanxi Provincial Department of Education (Grant No. 17JS052).

References

1. R. Fraenkel et al., "Cooled and uncooled infrared detectors for missile seekers," *Proc. SPIE* **9070**, 90700P (2014).
2. Z. Yuan, "New scheme of ship-borne IRSTS," *Infrared Laser Eng.* **38**(4), 583–588 (2009).
3. B. Shen and J. Chang, "Deformable mirror-based optical design of dynamic local athermal longwave infrared optic-al systems," *Opt. Lasers Eng.* **106**, 1–9 (2018).
4. Y. Nevo, "Dual-band optics," *Opt. Eng.* **52**(5), 053002 (2013).
5. C. Wang and Y. Wang, "Study of a borehole panoramic stereopair imaging system," *Int. J. Rock Mech. Min. Sci.* **104**, 174–181 (2018).
6. W. Zhenyu, "Optical design of panoramic system based on distributed aperture concept," *Appl. Opt.* **31**(2), 175–179 (2010).
7. L. Jun and L. Jing, "Design of five-channel infrared panoramic optical system," *Infrared Laser Eng.* **40**(4), 668–673 (2011).
8. P. M. McCulloch, C. Olson, and T. D. Goodman, "Eliminating Dewar narcissus artifacts induced by moving optics in infrared staring focal plane sensors," *Proc. SPIE* **8468**, 848606 (2012).
9. R. E. Fischer, B. Tadic-Galeb, and P. R. Yoder, *Optical System Design*, SPIE Press, Washington, Bellingham (2000).
10. M. Xia, H. Haiyong, and H. Kang, "Calculation method for airplane IR radiation and atmospheric transmittance," *J. Beijing Univ. Aeronaut. Astronaut.* **35**(10), 1228–1231 (2009).
11. Y. Nevo, D. Nir, and S. Wachtel, "Use of diffractive elements to improve IR optical systems," *Proc. SPIE* **4820**, 744–750 (2003).

Gao Ming is a doctor, professor, and doctoral supervisor. His current main research direction is photoelectric precision detection and photoelectric instruments, optical design theory and technology, and laser atmospheric transmission theory and technology.

Biographies of the other authors are not available.